ACS APPLIED MATERIALS & INTERFACES

Comment

Comment on "Bioinspired Reversible Switch between Underwater Superoleophobicity/Superaerophobicity and Oleophilicity/ Aerophilicity and Improved Antireflective Property on the Nanosecond Laser-Ablated Superhydrophobic Titanium Surfaces"

Peter Gregorčič*

Cite This: *ACS Appl. Mater. Interfaces* 2021, 13, 2117−2127

Read Online

ACCESS | Metrics & More | Article Recommendations | Supporting Information

ABSTRACT: Laser-textured surfaces enabling reversible wettability switching and improved optical properties are gaining importance in cutting-edge applications, including self-cleaning interfaces, tunable optical lenses, microfluidics, and lab-on-chip systems. Fabrication of such surfaces by combining nanosecond-laser texturing and low-temperature annealing of titanium Ti-6Al-4V alloy was demonstrated by Lian et al. in *ACS Appl. Mater. Inter.* **2020**, *12* (5), 6573−6580. However, it is difficult to agree with (*i*) their contradictory explanation of the wettability transition due to low-temperature annealing and (*ii*) their theoretical description of the optical behavior of the laser-textured titanium surface. This comment provides an alternative view—supported by both experimental results and theoretical investigation—on how the results by Lian et al. could be interpreted more correctly. The annealing experiments clarify that controlled contamination is crucial in obtaining consistent surface wettability alterations after low-temperature annealing. Annealing of laser-textured titanium at 100 °C in *contaminated* and *contaminant-free* furnaces leads to completely different wettability transitions. Analysis of the surface chemistry by XPS and ToF-SIMS reveals that (usually overlooked) contamination with hydrophobic polydimethylsiloxane (PDMS) may arise from the silicone components of the furnace. In this case, a homogeneous thin PDMS film over the entire surface results in water repellency (contact angle of 161° and roll-off angle of 15°). In contrast, annealing under the same conditions but in a contaminant-free furnace preserves the initial superhydrophilicity, whereas the annealing at 350 °C turns the hydrophobicity "off". The theoretical calculations of optical properties demonstrate that the laser-induced oxide layer formed during the laser texturing significantly influences the surface optical behavior. Consequently, the interference of light reflected by the air−oxide and the oxide−metal interfaces should not be neglected and enables several advanced approaches to exploit such optical properties.

KEYWORDS: *laser surface engineering, wettability, laser oxidation, thin-film interference, volatile organic compounds, polydimethylsiloxane, surface contamination*

■ INTRODUCTION

In their recent paper, Lian et al.[1] reported on the reversible wettability switch and decreased reflectivity of a titanium-alloy (Ti-6Al-4V) surface functionalized by nanosecond laser texturing. After the laser processing, the surface in question was additionally low-temperature annealed to achieve (i.e., to speed up) the superhydrophilic-to-superhydrophobic wettability transition. The authors demonstrated a reversible switch between two extreme wettabilities (super(oleo/aero)-philic and super(oleo/aero)-phobic) of their surface by applying ethanol to the surface or removing it by drying. With this, they ensured a transition between the Cassie and Wenzel wetting states on the laser-functionalized superhydrophobic surfaces during immersion into water. A similar Cassie−Wenzel transition on the laser-fabricated superhydrophobic surfaces has been demonstrated by using ultrasonic treatment in water.[2]

The results in ref 1 are undoubtedly important for applications with desirable switchable wettability, such as self-cleaning surfaces, tunable optical lenses, microfluidics, and lab-on-chip systems.[3] However, it is difficult to agree with (*i*) the contradictory explanation of the wettability transition that

happened during the low-temperature annealing and (*ii*) the theoretical description of the optical behavior of the laser-textured Ti-6Al-4V surface. Thus, this comment provides a discussion supported by results from the existing literature as well as supplementary experimental and theoretical investigation. In this way, it presents an alternative view of how the results in ref 1 should be correctly interpreted. Correct in-depth understanding of the experimental observations by Lian et al.[1] is of crucial importance for future implementation of the observed experimental findings into different applications including those at an industrial scale.
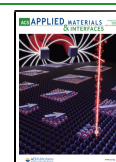
■ EXPERIMENTAL SECTION

Materials. Titanium-alloy samples with a thickness of 1 mm and dimensions of 20×20 mm^2 were used in the experiments. The samples were labeled as S1 and S2. The chemical composition of the samples was analyzed using an X-ray fluorescence spectrometer (Thermo Scientific Niton XL3t GOLDD+) and is shown in Table 1 together with

Table 1. Chemical Composition of the Titanium-Alloy Samples

	element (wt %)			
	Ti	Al	V	Fe
sample in this paper	89.3	6.2	4.3	0.16
sample by Lian et al.[1]	89.8	6.7	3.4	/

[a]The chemical composition of Lian et al.[1] was normalized to Ti, Al, and V elements (excluding oxygen) for a more consistent comparison (see also section S1 in the Supporting Information).

the chemical composition of the samples used by Lian et al.[1] The comparison confirms that both materials have a very similar elemental composition that can be classified as Ti-6Al-4V alloy (also known as TC4 and Ti64), which is the most widely used titanium alloy because of its high specific strength, stability at high temperatures, and good corrosion resistance.[4]

Laser Texturing. A nanosecond fiber laser (SPI Lasers Ltd., G4, SP-020P-A-HS-S-A-Y) irradiating pulses with a wavelength of 1060 nm at a repetition rate of 20 kHz was used to texture the samples. The pulse duration at full width at half-maximum (FWHM) and at 10% of the peak power equals 36 and 240 ns, respectively. A scanning velocity of 500 mm s^{-1}, average power of 10 W, and scanning line separation of 25 μm were used. The samples were textured in air atmosphere under ambient conditions. The processing parameters and their comparison with the parameters used by Lian et al.[1] are listed in Table 2.

Two samples labeled S1 and S2 were fabricated for the experiments using the exact same parameters.

Low-Temperature Annealing. Low-temperature annealing was performed in air atmosphere at normal pressure using the following three-step method (see also Figure S3 regarding the labeling of samples after each step):

- First, sample S1 was low-temperature annealed at 100 °C for 24 h in Furnace #1 (Kambič, model VS-50 SC). As revealed by the X-ray photoelectron spectroscopy (XPS) analysis and confirmed by the time-of-flight secondary ion mass spectroscopy (ToF-SIMS), the surface became contaminated after this annealing step because of the evaporation of silicon-containing compounds from the silicone components in this furnace (shown in Figure S1a), which are used as seals as Furnace #1 can also be used as a vacuum chamber (although not in this study). Thus, this furnace is described as *contaminated*. After this annealing step, the sample is labeled as S1.1.
- Secondly, sample S1.1 was additionally low-temperature annealed at 100 °C for 24 h in Furnace #2 (Binder, model FED56) *together* with a freshly made laser-textured sample S2. Because the XPS analysis of both samples after this annealing step has not revealed any additional contamination influencing the surface wettability, this furnace is described as *contaminant-free*. After this annealing step, the samples are labeled S1.2 and S2.2.

- The same samples S1.2 and S2.2 were also additionally annealed at 350 °C for 2 h (as suggested by Yang et al.[5]) in Furnace #3 (Nabertherm, model LT 9/11/B180), which can be heated up to 1100 °C. Thus, it can be cleaned of contaminants via preheating at high temperatures (above 500 °C). Because the wettability transition back to the superhydrophilic state indicates that no additional contamination occurred, this furnace is also described to be *contaminant-free*.

Wettability Characterization. The surface wettability was analyzed at room temperature using distilled water and a goniometer of our own design. The apparent contact angle was determined at six different locations on the surface from the images taken with a CMOS camera (XIMEA, MQ013MG-ON, 1.3 mega pixels). The contact angle was measured using a MathWorks MATLAB script, as described in ref 6. When applicable, the roll-off angle was also measured at eight different locations on each sample (see Table S3). The surface wettability was evaluated immediately after the laser processing (within 20 min) and immediately after each low-temperature annealing step (within 1 h; details are available in section S4 of the Supporting Information). If the water spread across the surface of the sample, such surface was classified as superhydrophilic and was considered to be in a saturated Wenzel state with a contact angle of zero degrees.[7−10]

TVOC Measurements. Some results in the literature suggest that the volatile organic compounds (VOC) play a significant role in the wettability transition after surface laser texturing.[11] Thus, the total volatile organic compounds concentration (TVOC) was measured using a PID-AH2 photoionization detector (Alphasense Ltd.), which detects the VOC with an ionization potential below 10.6 eV. The detector was calibrated using isobutylene and it was placed inside each of the three used furnaces at room temperature for more than 10 h (see the details in section S3 of the Supporting Information).

Surface Characterization. The chemical composition of the processed surfaces was analyzed using XPS performed with a PHI-TFA XPS spectrometer (Physical Electronics Inc.) equipped with Al-monochromatic source of X-rays. The surfaces were analyzed as prepared and additional survey spectra were acquired after 3 min of sputtering by 3 keV Ar$^+$ ions that removed approximately 3 nm of the top surface layer. The sputtered and the analyzed areas equaled 3×3 mm^2, and 0.4×0.4 mm^2, respectively. The samples were put into the XPS vacuum chamber within 3 h of their preparation. The deconvolution of the selected narrow-scan photopeaks is described in section S5 of the Supporting Information.

To confirm the surface contamination with PDMS, we additionally analyzed selected surfaces using the time-of-flight secondary ion mass spectroscopy (ToF-SIMS; TOF.SIMS 5 instrument, ION-TOF). The Bi$_3^+$ primary ions with 30 keV energy were used for the analysis. The secondary ions were acquired from the 0.2×0.2 mm^2 area, whereas the 2D maps were acquired on the 0.5×0.5 mm^2 regions with a resolution of 512×512 pixels.

■ INFLUENCE OF THE LOW-TEMPERATURE ANNEALING ON THE WETTABILITY TRANSITION

As shown by several authors,[7,12,13] the laser texturing of a metallic surface in an oxygen-containing atmosphere does not result only in modified surface topography but also in surface oxidation. On a microscopic scale, this manifests as a change of surface color[13,14] and results in modified surface wettability.[15−17] After the laser texturing, the surfaces may become superhydrophilic in a saturated Wenzel regime ($\theta = 0°$).[7−10]

Table 2. Comparison of the Laser-Processing Parameters in This Study and in the Study by Lian et al.[1]

	wavelength (nm)	pulse duration	repetition rate (kHz)	scanning speed (m s^{-1})	average power (W)	scanning line separation (μm)	beam waist diameter (μm)
parameters in this paper	1060	32 ns at FWHM, 240 ns at 10%	20	500	10	25	38
parameters by Lian et al.[1]	1064	100 ns	20	500	12	25	data not available

However, this regime is not stable and the superhydrophilic-to-superhydrophobic transition usually occurs over the course of several weeks or months if these surfaces are exposed to atmospheric air.[2,6,15,17] Although the underlying mechanisms for this transition are still under debate,[18] several experimental observations[5,19−22] convincingly endorse contamination as one of the most likely reasons.

Lian et al.[1] reported that they sped up the wettability transition by the low-temperature annealing carried out for 24 h at 100 °C. They explained this by stating: "It is well known that the laser-ablated surfaces have a superhydrophobic property after low-temperature annealing /.../[5,20,21]" They also emphasized this inconsistent explanation in their conclusions: "After nanosecond laser ablation and low-temperature annealing treatments, the resultant titanium surface had superhydrophobicity."

The papers by Long et al.[20] and Yang et al.[5] that Lian et al.[1] cited to support their (above listed) statements actually showed just the *opposite.* Both cited studies used low-temperature annealing to *switch off* the developed hydrophobicity and to return the aged (already superhydrophobic) laser-textured surfaces into the initial superhydrophilic (i.e., saturated Wenzel[7−9]) regime. From an application point of view, the influence of the low-temperature annealing on the wettability transition of laser-textured surfaces is important. Thus, it is worth clarifying these at first sight *contradictory* reports in the literature.

Influence of the Contamination by Organic Compounds. Long et al. have shown that the wettability transition after laser processing of copper[19] and aluminum[20] remarkably depends on the atmosphere, in which the processed surfaces are stored. Similar behavior was observed by Yan et al.[22] for laser-textured brass, which was exposed to different media (including liquids) after processing. They *all* found that the organic-rich environments significantly shorten the time needed for the transition toward (super)hydrophobicity. Their XPS analyses revealed a strong correlation between the high contact angles and the increased C-to-metal ratios. Additionally, it was convincingly shown[5,19,20] that low-temperature annealing (in the range of 250−350 °C) *recovers* the initial (super)-hydrophilicity and decreases the C-to-metal ratios, because low-temperature annealing desorbs the low-surface-energy monolayer.[23] This is just *the opposite* observation as reported in ref 1.

However, very similar—and at first sight contradictory—results to those reported by Lian et al.,[1] where the low-temperature annealing promotes superhydrophobicity were also published by Chun et al.[24] and Ngo et al.[25] It is worth mentioning that both papers were published by the same group, but unfortunately, neither of them contains detailed information regarding surface chemistry. The XPS analysis by Lian et al.[1] (Figures S3a, b in the Supporting Information of ref 1) clearly indicates that the C/Ti ratio significantly *increased* (more than 2-fold) after their low-temperature annealing (from 0.7 before the annealing to 1.7 after the annealing). This confirms that their annealing happened in a furnace and/or laboratory *contaminated* by organic compounds. Such an explanation would be consistent with several reports in the literature showing that hydrophilic-to-hydrophobic transition is promoted by the surface exposure to the organic-rich[5,19,20,22] or even "vacuum" environments.[19,21]

It has been convincingly demonstrated by Yan et al.[26] that even a "vacuum" environment may promote the hydrophilic-to-hydrophobic transition due to the chemisorption of organic

molecules (e.g., oil droplets) from vacuum pumps. They clearly confirmed this by their observation of significantly accelerated development of superhydrophobicity on Fe_2O_3 nanoflake films. When these nanoflake films were exposed to vacuum, the contact angle increased to $\theta = 160°$, whereas the same samples stored in a nitrogen atmosphere kept the initial contact angle of $\theta = 0°$. All of this leads to the conclusion that the organic compounds in the atmosphere, which the samples are exposed to, crucially determine the hydrophilic-to-hydrophobic transition.

From the existing literature, it also follows that (super)-hydrophilic-to-(super)hydrophobic transition under ambient conditions happens on a multitude of laser-textured metals and metal alloys with different chemical and catalytic activity as well as different crystallographic structure.[18] The samples in these studies were textured by a wide range of laser-pulse durations, including nanosecond,[6,7,16,17,27] picosecond,[20] and femtosecond pulses.[2,15] Moreover, a similar transition has been observed on surfaces oxidized by oxygen plasma treatment,[28] reactive magnetron sputtering,[29] and even ionizing (gamma) radiation.[30] All of this clearly indicates that the mechanisms of the wettability transition after surface oxidation should be universal and should not characteristically depend on a specific metal, metal alloy or even the processing approach and fabrication parameters, as already pointed out by Boinovich et al.[18]

Wettability Transition due to Low-Temperature Annealing. As has been explained above, the wettability transition toward hydrophobicity most probably happens because surface contamination with different hydrophobic compounds stemming from the atmosphere. This has also most likely happened in the study by Lian et al.[1] as indicated by the increased C 1s peak in their survey XPS spectrum in comparison with the XPS spectrum they acquired after laser texturing and before annealing. Their Supporting Information reveals that the C/Ti ratio is more than doubled after the annealing. Unfortunately, they have not measured and/or showed the narrow-scan XPS photopeak for C 1s. This is necessary to reveal the C−C/C−H concentration that is, because of the nonpolar bond, usually recognized as the most probable reason for the increased hydrophobicity in contamination with organic compounds.[5,19,20] However, as shown by the experiments in this study, they are not the only possible reason for the contamination during annealing.

To demonstrate this, we textured two Ti-6Al-4V samples (labeled S1 and S2) with a chemical composition very similar to that of the sample used in ref 1 (see Table 1) by using similar laser-processing parameters as Lian et al.[1] (see Table 2). According to the reasons explained in the previous subsection, it is worth believing that slight deviations of the processing parameters in both experiments should not significantly influence on the final result in terms of the wettability transition.

Immediately after the laser texturing, the surfaces were in a saturated Wenzel regime[7,8,10] with $\theta = 0°$, as clearly evident from Figure 1a, b (see also Figure S4). When the hydrophilic solid surface is sufficiently rough, the liquid wicking may lead to its complete homogeneous wetting resulting in the saturated Wenzel regime, where the water droplet transforms into a thin film with a contact angle of zero degrees.[9] In such cases, different surface wettabilities cannot be evaluated through the contact angle anymore, but other approaches such as measuring the wicked volume flux[31] or droplet spreading[32] should be used to distinguish wettability variations between individual surfaces.
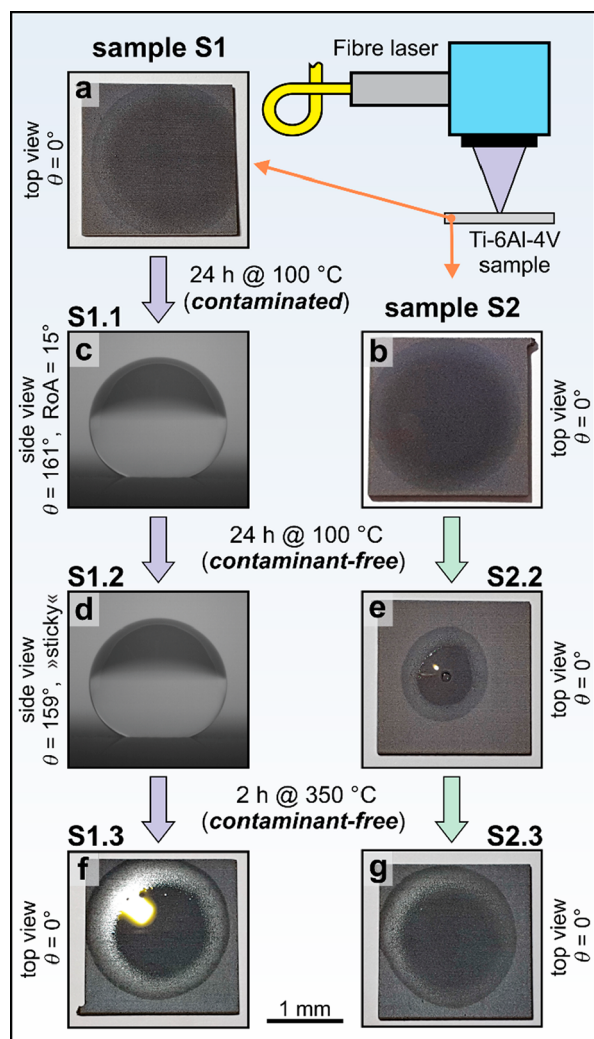
Figure 1. Wettability of the laser-textured Ti-6Al-4V samples. (a) S1 and (b) S2 immediately after the laser texturing. (c) S1.1 after 24 h of annealing at 100 °C in contaminated Furnace #1. (d) S1.2 and (e) S2.2 after an additional 24 h of annealing at 100 °C in contaminant-free Furnace #2. (f) S1.3 and (g) S2.3 after an additional 2 h of annealing at 350 °C in contaminant-free Furnace #3. Panels a, b, e, f, and g show the top view, acquired 2 s after the contact between the water droplet and the surface, wheras panels c and d show the side view. The same scale shown at the bottom applies to all images.

Thus, the images showing the droplet spreading are provided in Supporting Information (Figures S4, S7, S8, S11, and S12).

After annealing in a *contaminated* Furnace #1 (24 h at 100 °C), the contact (CA) and roll-off (RoA) angle of sample S1.1 (Figure 1c) equaled to $\theta = 161.2° \pm 4.6°$ and RoA = $15.3° \pm 5°$, respectively (Figure S5 and Tables S2 and S3). The same experiment was repeated approximately two months later and gave very similar results (see section S4 in the Supporting Information).

In the second annealing step, the already hydrophobic S1.1 and freshly textured superhydrophilic S2 samples were annealed *together* in the *contaminant-free* Furnace #2 (24 h at 100 °C). Sample S1.2 was still hydrophobic with a similar contact angle as before this annealing step ($\theta = 159.3° \pm 2.2°$), but its surface became significantly more "sticky" (Figure 1d). The RoA was measured at eight locations; in five cases, there was no RoA (>90°), whereas for the other three cases, the results were in the range of 30−80° (see also Figure S9 and Tables S2 and S3). As

shown in Figure S10 and by data in Tables S2 and S3, the same trend is observed in the experiments repeated two months later. Conversely, initially superhydrophilic sample S2.2 stays super-hydrophilic (Figure 1e; $\theta = 0°$), but the transition of the water droplet into a water film after the annealing was slower than immediately after the laser texturing (Figures S7 and S8). This most likely happened due to cross-contamination between samples S1.1 and S2.1 as they were annealed together.

In the third step, samples S1.2 and S2.2 were again low-temperature annealed in a *contaminant-free* Furnace #3 for additional 2 h at 350 °C, as suggested by Yang et al.[5] As expected, the low-temperature annealing at a higher temperature *recovered* the initial saturated Wenzel state (Figures 1f, g and Figures S11 and S12), which is consistent with the results by Long et al.[19,20] and Yang et al.[5]

To summarize, the wettability evaluation clearly shows that annealing at 100 °C leads to a hydrophobic surface *only* when done in a *contaminated* environment. Otherwise, it does not contribute to the superhydrophilic-to-superhydrophobic transition of the (laser-textured) samples. However, annealing at 350 °C turns the hydrophobicity off and recovers the initial superhydrophilicity.

Surface-Chemistry Characterization and Discussion of the Wettability Transition. The presented annealing experiments show that contradictory results in the terms of wettability transition may be observed at the *same* annealing temperature and for the *same* annealing duration, but in *different* furnaces (i.e., annealing environments). This is a clear indicator that this transition is governed by environmental contamination. However, the sources of surface contamination (when not intentionally provided) are difficult to identify. An important reason for this is that just a few molecular layers (or even a monolayer) of contaminant may already completely change the surface energy and, consequently, surface wettability.[33]

To identify the source(s) of (unintentional) contamination in Furnace #1 used in the supplementary experiments, we analyzed the surface chemistry after each step of sample processing using XPS (Figure 2 and section S5 in the Supporting Information). All XPS spectra are calibrated by the C 1s peak at 284.6 eV and deconvoluted as described in the Supporting Information. The narrow scans of the Ti 2p, N 1s, O 1s, C 1s, and Si 2p spectra were normalized by the Ti 2p intensity and are shown in Figure 2.

The Ti 2p spectra with two peaks at 458.9 eV (Ti $2p_{3/2}$) and 464.7 eV (Ti $2p_{1/2}$) indicate that the surface is covered with TiO_2[34] after laser texturing and that the titanium-oxide chemical composition does not significantly change during the annealing steps. The photopeak at 407.3 eV in the N 1s spectrum shows that NO_3 is adsorbed on the surface[35] of the laser-textured (S1) sample (the black curve in Figure 2b, see also Figure S24). The NO_3 most probably arises from the optical breakdown during the laser texturing, where the interaction between the laser-pulse and surface leads to ionization of the textured solid and surrounding air, consequently resulting in plasma formation. However, this photopeak disappears after the annealing (the red and the green curves in Figure 2b).

It is generally accepted that due to their strong affinity to water, superhydrophilic surfaces adsorb at least a monolayer of water when exposed to atmospheric air.[10] This is visible on the O 1s spectrum of the laser-textured (S1) sample (the black curve in Figure 2c, see also Figure S18) from the shoulder centered at the characteristic binding energy for water molecules adsorbed to TiO_2 (533.5 eV).[35,36] When water is present on a hydrophilic
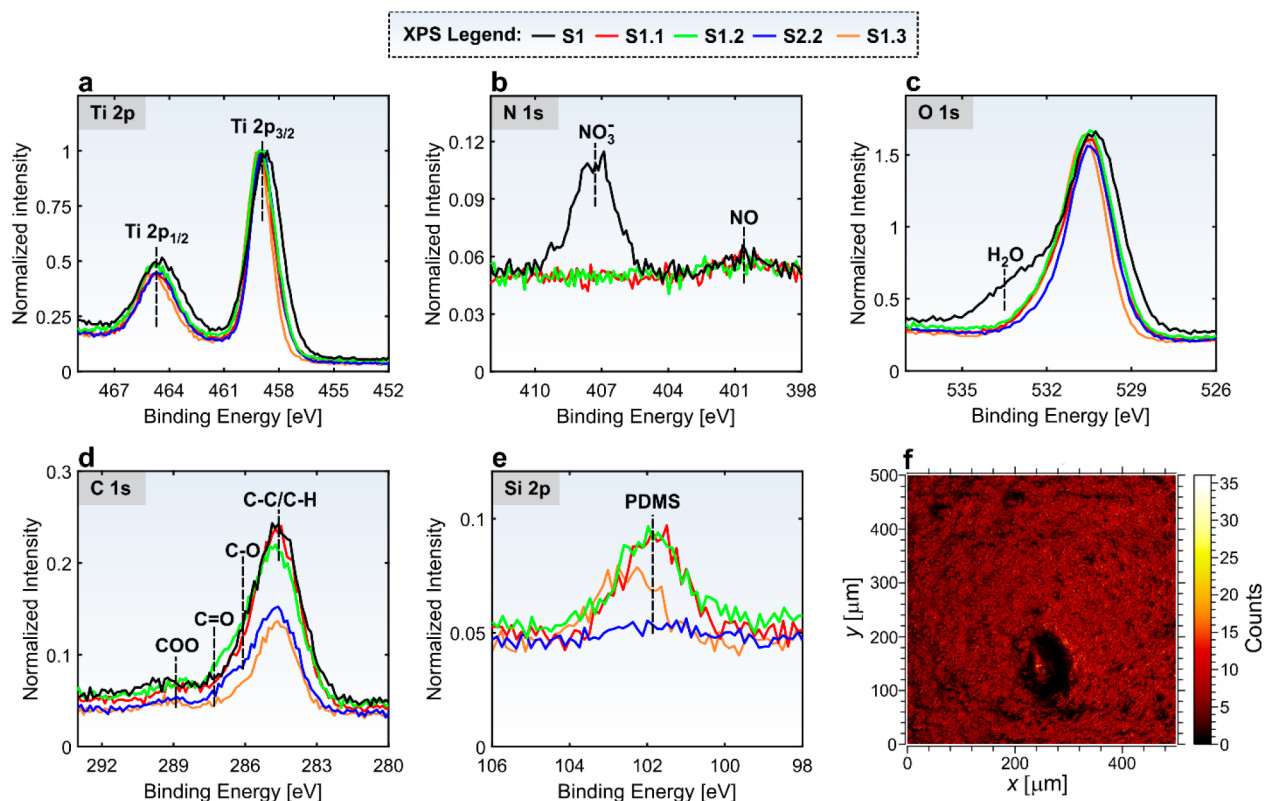
Figure 2. XPS spectra of (a) Ti 2p (normalized by itself) and (b) N 1s, (c) O 1s, (d) C 1s, and (e) Si 2p normalized by Ti 2p intensity. (f) ToF-SIMS 2D map showing the integrated intensity of the $Si_3C_5H_{15}O_3^+$, $Si_2C_5H_{15}O^+$, and $SiC_3H_9^+$ secondary ions on sample S1.1.

surface, the adsorption of hydrophobic contaminants is prevented or at least slowed down.[10] However, this layer of water also attracts volatile organic compounds, which are always present in the laboratory environment (e.g., they come from the exhaled air[37,38]) and can, when in sufficient quantities, destabilize the water film, leading to the "naked" exposure of the hydrophilic surface to the contaminated atmosphere.[10] When the samples are annealed at temperatures around or above the boiling point of water, the water layer is destabilized and dries out because of evaporation. Thus, the shoulder in the O 1s photopeak (characteristic for adsorbed water) disappears on all annealed samples (the red, green, blue, and orange curves in Figure 2c).

Several studies have shown a strong correlation between the structures with nonpolar C–C or C–H bonds and the hydrophobicity of the adsorbate.[5,11,19,20] Thus, the C 1s peaks were deconvoluted to the hydrocarbon chains and graphitic structure (C–C/C–H, positioned at 284.6 eV) and the following three polar functional groups incurring hydrophilicity: alcohol/ether group (C–O with binding energy +1.5 eV from the main peak), aldehydes/ketones (C=O with binding energy +2.7 eV from the main peak) and carboxyl/ester group (O–C= O with binding energy +4.3 eV from the main peak).[19] The concentrations of the C–C/C–H in the C 1s peak are shown and directly compared against the measured contact and roll-off angles in Table S5 (see also Figures S19–S23). The results do not show any significant correlation between the C–C/C–H concentrations and hydrophobicity for the presented annealing experiments. This is most probably because of too short exposures to the atmospheric air and the involvement of other contaminants, as explained below. However, it is evident that annealing at temperatures above 300 °C in contaminant-free

furnaces decreases the C–C/C–H content (Figure 2d and Table S5) and the C/Ti ratio (Table S6), which is consistent with other reports in the literature.[5,19,20] The C/Ti ratio immediately after the laser texturing equals 0.8, which is very similar to the value obtained by Lian et al.,[1] who reported the C/ Ti ratio after laser texturing (and before annealing) of 0.7.

Some authors[11] also suggest that the hydrophobicity on the laser-textured surfaces develops due to VOC adsorption. Thus, TVOC were measured in all three furnaces at room temperature (unfortunately, the used sensor cannot operate at temperatures above 55 °C) 1 day after the annealing experiments. Interestingly, the results in Figure S2 show significantly lower VOC concentrations in Furnace #1 leading to hydrophobicity as in Furnaces #2 and #3 that do not enhance water repellency. Moreover, even the C content on the samples (see Table S4) does not correlate well with the TVOC concentration measured at room temperature. These findings suggest that when performing the annealing at temperatures well-above the room temperature and due to relatively short exposures of the samples to the atmospheric air (for only 24 h), the TVOC concentration (at least when not extreme) may not play the same crucial role as in the case of longer exposure to contaminated air (e.g., 3 months in ref 11 or 8–30 days in refs 19 and 20). While one of the important roles of VOC is destabilization of the water film protecting the surface against hydrophobic contaminants,[10] this role is most likely not as decisive during annealing processes, as the water film is already destabilized because of high temperatures. However, it would be very interesting to further investigate the mechanisms proposed in ref 11 under the annealing conditions.

After the first annealing step in the contaminated Furnace #1, the Si 2p peak, which was not present on sample S1 (see Figure
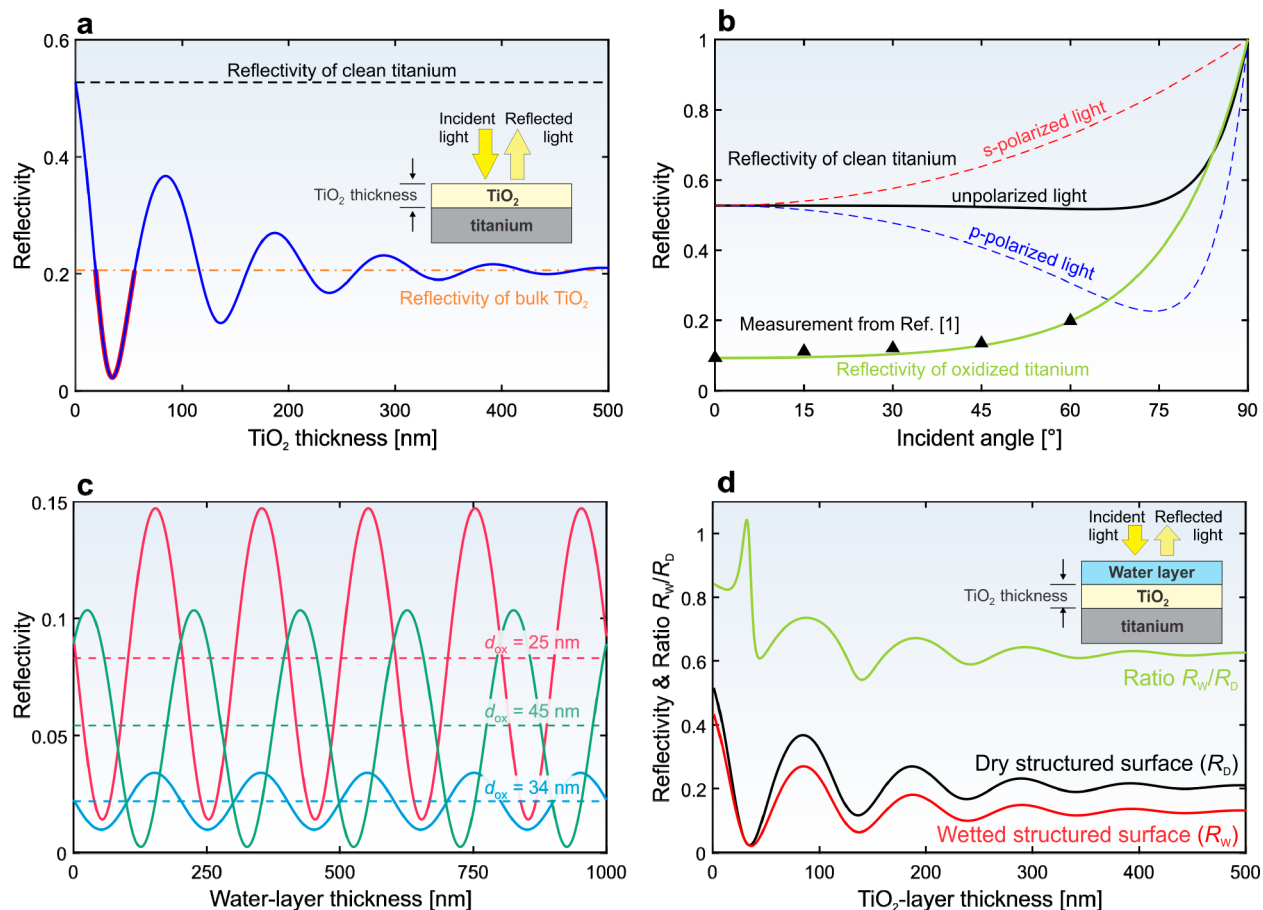
Figure 3. Supplementary theoretical calculations. (a) Influence of the TiO_2 thickness on the reflectivity of a titanium surface. (b) Theoretical reflectivity of clean titanium (for the p-, s-, and unpolarized light) and theoretical reflectivity for the oxidized titanium (d_{ox} = 25 nm) as a function of the incidence angle; measurements from ref.[1] are shown as black triangles. (c) Reflectivity of titanium covered by a TiO_2 layer and water as a function of the water-layer thickness; results for three different oxide thicknesses d_{ox} are shown and the dashed curves present the average reflectivity. (d) Reflectivity as a function of the oxide layer thickness for a dry sample (only oxide is present on a titanium surface, the black curve) and for a wet sample (the oxide is additionally covered by water, the red curve). The green curve shows the ratio between the red and the black curves. Unless explicitly stated otherwise, calculations are made for λ = 532 nm and for normal incidence (θ_i = 0°) of unpolarized light.

S13 and Table S4), appears on sample S1.1 (the red curve in Figure 2e). Its position at 101.8 eV perfectly corresponds to the hydrophobic silicon-based organic polymer PDMS.[39,40] No other Si compounds are visible in the Si photopeaks (Figures S25−S27). This PDMS contamination most probably arises from the silicone components of Furnace #1 (Figure S1a), as it has been shown that dimethylsiloxane polymers evaporate even at temperatures below 80 °C.[41]

Contamination of surface S1.1 with PDMS is additionally confirmed by ToF-SIMS analysis. Figure 2f shows the ToF-SIMS 2D map of the integrated intensity of the $Si_3C_5H_{15}O_3^+$, $Si_2C_5H_{15}O^+$, and $SiC_3H_9^+$ secondary ions. It is evident that the sample S1.1 is homogeneously covered by a thin PDMS layer (see also Figure S29).

The PDMS peak is also clearly observed in the XPS signal, acquired on the sample S1.2 (the green curve in Figure 2e). The Si concentrations, estimated from the survey spectrum recorded on sample S1.2 and listed in Table S4, show a slight decrease in the Si concentration after annealing in Furnace #2. This may explain why the S1.2 surface became sticky, as seen from Figure 1 and Table S3. However, such small concentrations from the survey spectrum acquired on rough surfaces (where the XPS signal from the valleys is weaker than from the tops and where the sputtering is not able to remove the same layer thickness

from the tops and the valleys of the rough surface) should be interpreted with caution. Thus, further investigation beyond the scope of this comment is needed to fully understand the desorption of the thin PDMS film at temperatures around 100 °C.

A significantly smaller Si 2p photopeak than for samples S1.1 and S1.2 is observed on sample S2.2 (the blue curve in Figure S2e). This confirms that cross-contamination occurred, as samples S1.1 and S2 were annealed together in Furnace #2. A small amount of PDMS explains the decreased wickability of the still-superhydrophilic sample S2.2 (see Figure S7).

Annealing at 350 °C in Furnace #3 turned the hydrophobicity off and returned the S1.3 sample into the initial superhydrophilic state (Figure 1f). This is consistent with previous observations that annealing at temperatures above 350 °C leads to PDMS pyrolytic degradation to oxide films.[42] As it is observable from the position of the orange curve in Figure 2e (see also Figure S28), the Si 2p peak is shifted toward higher binding energies (102.5 eV), but not completely to SiO_2 value (103.3 eV). This indicates that the PDMS is oxidized toward SiO_2.[40] Oxidation of the PDMS film on the sample S1.1 after annealing at 350 °C in Furnace #3 is additionally confirmed by ToF-SIMS analysis. This is evident from the comparison of the normalized

intensities for the selected Si-containing secondary ions on surfaces S1.1 and S1.3 (Table S7).

Switched-off hydrophobicity of the PDMS coated surfaces has also been observed by Yuan et al.[43] They turned the hydrophobic properties of the PDMS coating off by annealing the samples at 390 °C. In doing so, they demonstrated a high degree of switchability in the wetting behavior (i.e., between superhydrophobic and superhydrophilic states) of the PDMS-coated surfaces.

To summarize, the presented supplementary experiments clarify that annealing at 100 °C may *conserve* surface hydrophilicity (when performing the annealing in an uncontaminated atmosphere) or it may *promote* the wettability transition toward hydrophobicity in the presence of the hydrophobic contaminants (in case of using the contaminated Furnace #1 and in the experiments performed by Lian et al.[1]). This explains that contradictory results by Lian et al.[1] were observed, as the authors did not appropriately control the contamination of the atmosphere in their furnace. Their XPS measurements clearly support this explanation.

However, as revealed by the presented supplementary experiments, the surface contamination during the low-temperature annealing may not arise only from the hydrocarbon contamination, as the silicone components of the furnaces may be an additional and usually overlooked source of low-surface-energy contaminants. This is especially problematic in furnaces with maximum temperatures up to 200 °C, because they may contain silicone parts (such as seals and tubes for vacuum or gas atmospheres) that are not present in the furnaces allowing higher temperatures (where PDMS degrades) because of the temperature limitations of silicone. As shown by the annealing experiments in Furnace #3, the contamination can be reduced by performing the annealing at 350 °C. In this context, preheating of the furnace to high-enough temperatures can be used to ensure contaminant-free annealing by degrading the contaminants before the annealing process. Furthermore, alternating the low-temperature annealing process in *contaminated* and *contaminant-free* furnaces may represent an additional alternative method to achieve the reversibly switched wettability. In case of PDMS contamination, this is of additional importance, because the PDMS is known as an inert, nontoxic, and biocompatible material.[44] Consequently, such approach to reversibly switching the surface wettability by annealing in an (intentionally) PDMS-enriched atmosphere could be utilized in biomedical applications.

REFLECTIVITY OF THE LASER-TEXTURED METALLIC SURFACES

Lian et al.[1] also reported a modification of reflectivity of the laser-textured titanium samples, but their theoretical explanation is incorrect for several reasons:

- During their experimentation, they used unpolarized light, but the theoretical curve in Figure 5c from ref 1 explains the measured dependence of the reflectivity as a function of the incident angle by using the equation that is valid *only* for the s-polarization (called also TE). For this reason, the shape of their theoretical description (when analyzed carefully) does not correspond to the measured data (compared in Figure 3b and showing the shape of this dependence for s- and p-polarized as well as unpolarized light).

- They neglected that titanium is a metal, not dielectric. Because metals are conductive, they attenuate the electromagnetic waves. As it is widely known[45] and explained in the Supporting Information, strong absorptivity of metals is *inevitably* accompanied by high reflectivity. Thus, the complex index of refraction ($\hat{n} = n + i\kappa$) should be used instead of the real one. For metals, the imaginary part (i.e., the extinction coefficient κ) is preponderant and, consequently, should not be neglected.

- They neglected the oxide film that forms on titanium due to its strong affinity to oxygen. When exposed to air, titanium is covered by a several nanometers thick oxide film.[46] This film becomes even thicker during laser texturing because of the high temperatures induced by laser ablation.[47] As shown by the XPS measurements (Figure 2a), the titanium surface after laser texturing is completely covered by TiO_2. The oxide film significantly influences the optical properties of the titanium surface (see Figure 3a).

- Figures 5a, b in ref 1 and the accompanying discussion neglect the interference between the light reflected from the air−water, water−oxide, and oxide−titanium interfaces. It is well-known that in case of thin films (with thicknesses up to several hundred nanometers), the interference *should not* be neglected even for the conventional light sources (classified as "incoherent" sources). The most-known manifestation of this phenomenon are multiple colors appearing on a soap bubble or on an oil film floating on water because of light reflections.

The following theoretical investigation shows, how the results in ref.[1] related to the optical properties of the laser-functionalized titanium surfaces are correctly interpreted. This is demonstrated by supplementary theoretical calculations, shown in Figure 3 and explained in details in sections S7−S9 of the Supporting Information. For the sake of this demonstration, the measured results in ref 1 were digitalized by appropriate image processing.

Reflectivity of the Titanium Surface. As reviewed in the Supporting Information, several authors[46,48−50] have measured the refractive index of pure titanium as a function of the wavelength. The reflectance for the normal incidence ($\theta_i = 0$) in air is calculated as

$$R_{normal} = \frac{(n_0 - n)^2 + \kappa^2}{(n_0 + n)^2 + \kappa^2} \tag{1}$$

where $n_0 = 1$ stands for the refractive index of air, whereas $n = n(\lambda)$ and $\kappa = \kappa(\lambda)$ are the wavelength-dependent real and imaginary parts of the refractive index $\hat{n}$, respectively. A comparison between the data in the literature and the measured spectrum for the unprocessed surface (taken from Figure 4c in ref.[1]) is made in Figure S30. As it is evident from Figure S30b, the most similar reflectivity is obtained by using the refractive index measured by Mash and Motulevich.[49] Thus, these data are used for supplementary calculations supporting this comment.

The average reflectivity (for wavelengths in the range of 400−1000 nm) calculated from ref 49 (the dark green curve in Figure S30a) equals 0.55, whereas the average reflectivity, measured by Lian et al.[1] (the black curve in Figure S30) equals 0.41. There are several reasons for this difference. The refractive index in ref 49 was measured on pure titanium (99.99%) and special care was taken to minimize the surface oxidation. On the contrary, the sample in ref 1 is an alloy with a titanium content of

approximately 90% (see Table 1) and was covered by an oxide layer even before the laser texturing process because of natural oxidation. Additionally, the surface was most likely not perfectly smooth and had some degree of roughness.

Influence of the Oxide Layer on Surface Reflectivity. The effect of the oxide layer on the reflectivity at a wavelength of 532 nm and for normal incidence of the unpolarized light is shown in Figure 3a. Here, the refractive index for titanium of $\hat{n}_{Ti}$ (532 nm) = 2.21 + i2.90 (taken from ref 49) and the refractive index for TiO$_2$ of $\hat{n}_{TiO_2}$ (532 nm) = 2.6 + i0.37 (taken from ref 51) are used. The results in Figure 3a are obtained by calculating the reflectivity for the electric field, when the metal is covered by a single thin film (STF):[51]

$$r_{STF} = \frac{r_{12} + r_{23}e^{i\delta_{ox}}}{1 + r_{12}r_{23}e^{i\delta_{ox}}} \qquad (2)$$

As explained in the Supporting Information, the r_{ij} in eq 2 stands for the electric field reflectivity (Fresnel equations for the s- and p-polarization (eqs S3 and S4)) on the $i-j$ interface (1 denotes air, 2 is TiO$_2$, and 3 denotes titanium; see Figure S31), whereas the intensity (or power) reflectivity is calculated as $R = r_{STF} r_{STF}^*$, where the asterisk denotes the complex conjugate. In case of unpolarized light, the intensity reflectance is the arithmetic mean of the intensity reflectance for the p- and s-polarizations (see eq S8).

The phase change shift of light passing through the oxide film is calculated as $\delta_{ox} = \frac{4\pi d_{ox}}{\lambda}\hat{n}_{ox}\cos(\theta_{ox})$, where d_{ox} denotes the TiO$_2$ thickness, θ_{ox} is the angle of light propagation inside TiO$_2$ (see Figure S31), and λ is the light wavelength in vacuum. As demonstrated in section S8 in the Supporting Information, when the complex refractive index $\hat{n}_{ox}$ is used in δ_{ox}, the extinction coefficient in the exponential term of eq 2 appropriately describes the light absorption in the thin film (the real part in eq S17).

As clearly visible from Figure 3a, the reflectivity as a function of the oxide thickness goes from 0.53 as for the clean titanium (the black dashed line in Figure 3a) and reaches its minimum at 0.023 when the oxide thickness equals 34 nm. For an oxide thickness exceeding 0.5 μm, the reflectivity stabilizes at 0.206. This happens because of the complex refractive index of TiO$_2$ used in the calculation. Consequently, the extinction coefficient in phase change δ_{ox} in eq 2 contributes to the absorption (see the explanation in eqs S15−S17) already within submicrometer-thin oxide layer, because $\kappa_{TiO2} = 0.37$ gives the absorption length of 114 nm. Here, the absorption length (i.e., the inverse Lambert absorption coefficient) equals the length, where the $(1 - e^{-1}) = 63\%$ of the light power is absorbed. Thus, when the oxide layer becomes thicker, the titanium surface is not "visible" by the incident light anymore. For this reason, calculations using eq 2 for thick TiO$_2$ layer result in a similar value to the reflection from the bulk TiO$_2$, calculated by eq 1, which gives the reflectivity of 0.206 (shown by the dash-dotted orange line in Figure 3a).

Lian et al.[1] reported that the reflectivity of their titanium surfaces after texturing decreases to 0.092. They explained this as the influence of the surface micro- and nanostructures. However, it is evident from Figure 3a (the red-highlighted region) that a similar effect will be observed, if the laser ablation leads to a modified oxide thickness in the range of 19−55 nm. Most likely, both effects, that is the modified surface topography and the oxidation (i.e., the modified surface chemistry), contribute to the decreased reflectivity after laser texturing.

However, as clearly demonstrated by the theoretical results in Figure 3a, the influence of the interference effects on the oxide layer should not be neglected and must be appropriately evaluated.

Reflectivity of the Oxidized Titanium as a Function of the Incident Angle. Lian et al.[1] measured the reflectivity of the laser-textured titanium as a function of the incident angle (the black triangles in Figure 3b). They used the *wrong* theoretical explanation of this behavior. Moreover, this wrong calculation included the wrong refractive index of titanium, as they completely neglected the extinction coefficient. Thus, similar values between their theoretical calculation and the measured reflectivity were just a *coincidence*.

The theoretically calculated reflectivity of titanium should give similar results as the measured reflectivity on flat (unprocessed) titanium. This happens if the correct refractive index is used, as clearly observable from Figure 3b, where the theoretical reflectivity for the p-, s-, and unpolarized light is shown for $\lambda = 532$ nm. However, observations in ref 1 should also be explained in the context of surface oxidation.

If a 25 nm thick TiO$_2$ layer is assumed (as suggested from the theoretical results in Figure 3a), the theoretical curve for the unpolarized light (eq 2) corresponds well with the measurements (the green curve in Figure 3b). However, to further distinguish between the contributions of the surface roughness and the oxide layer on the optical properties, additional surface analyses (not available in ref 1) would be required. Such analyses should include (i) the XPS characterization of the surface oxides (only the survey provided in ref 1 is not enough, because narrow scans—similar to those in Figure 2a—and corresponding deconvolutions are needed to identify different types of titanium oxides), and (ii) the evaluation of the oxide thickness, including the oxide-thickness variation (e.g., by using combination of FIB and SEM). Nevertheless, the supplementary theoretical calculations presented in this comment clearly show that the interference effects due to titanium oxidation should not be neglected.

Influence of Surface Wetting on Surface Optical Properties. Lian et al.[1] report that the reflectivity changes when the surface is wet (i.e., covered by a thin film of water). Again, they neglected the interference effects even though—as evident from the theoretical calculations in Figure 3a, d—they should not be neglected. As explained in the section S9 of the Supporting Information, the reflectivity for an electric field in case of a double thin-film layer (DTF) system can be calculated as[14]

$$r_{DTF} = \frac{r_{12} + r_{23}e^{i\delta_w} + r_{34}e^{i(\delta_w+\delta_{ox})} + r_{12}r_{23}r_{34}e^{i\delta_{ox}}}{1 + r_{12}r_{23}e^{i\delta_w} + r_{12}r_{34}e^{i(\delta_w+\delta_{ox})} + r_{23}r_{34}e^{i\delta_{ox}}} \qquad (3)$$

where indices 1, 2, 3, and 4 stand for air, water, TiO$_2$, and titanium, respectively (see Figure S32), and the phase change due to light propagation in water δ_w is calculated similarly as phase change due to light propagation within the oxide film in eq 2.

The refractive index of water in the visible spectrum is real ($n = 1.33$), since its absorption is negligible (especially in case of thin films).[52] Using the value of $\kappa = 0$ ($\kappa = 1.5 \times 10^{-9}$ at 532 nm,[52] which gives an absorption length of 28 m and can be safely neglected) in eq 3 does not result in any light attenuation within the water film. Consequently, the amplitude in the modified reflectivity due to altered thickness of the water layer is constant (see Figure 3c for three different (fixed) thicknesses of TiO$_2$

layer). As evident from the results in Figure 3c, the period in the reflectivity is below 250 nm ($<\lambda/2$) when the thickness of the water layer is changing. The results in ref 1 indicate that the surface roughness after the laser texturing is in the micrometer range. Thus, the water layer thickness on the sample (when in the superhydrophilic state) also changes within the micrometer range. Consequently, the surface reflectivity can be averaged for different thicknesses of the water layer (the dashed lines in Figure 3c).

Lian et al.[1] measured that the reflectivity of the wet textured surface is always lower than the reflectivity of the dry structured surface. They demonstrated that this can be used for the switched optical properties, which is important from the application point of view. Their (fair) experimental observation can be correctly explained by the interference effect in the double thin-layer system (Figure 3d). The calculations of the reflectivity as a function of the TiO_2 thickness for a dry sample (eq 2 and the black curve in Figure 3d, denoted by R_D) and for a wet sample (eq 3 and the red curve in Figure 3d, denoted by R_W) show that this is true for almost all oxide layer thicknesses. The ratio R_W/R_D (the green curve in Figure 2d) is above unity only if the oxide thickness is in the range of 29.5−33.5 nm; otherwise, it is always lower than 1, which agrees well with the experimental observations by Lian et al.[1] Calculations in Figure 3d are made by using the averaged values (the dashed lines in Figure 3c) for different thicknesses of the water layer, as is justified by the explanation in the previous paragraph.

The results in ref 1 additionally show that the difference in the reflectance between the dry and the wet textured surface changes with varying scanning line separation used in laser texturing. The theoretical result in Figure 3d suggests that this might happen because different processing parameters lead to oxide layers with different thicknesses. Thus, it would be worth measuring the oxide thickness after texturing using different scanning lines separations to compare the measured values with the results in Figure 3d.

CONCLUDING REMARKS

Undoubtedly, laser texturing of metallic surfaces represents a promising, straightforward, scalable, and chemical-free method for fabrication of bioinspired surfaces with reversibly switchable wettability and modified optical properties. However, advanced approaches to exploit these switchable properties require correct and in-depth understanding of (*i*) the wettability transition during the low-temperature annealing and (*ii*) the light reflection on laser-textured (oxidized) metallic surfaces. In this context, the presented discussion of the already published results and the supplementary experiments clarify that controlled contamination is crucial in obtaining consistent surface wettability alterations after low temperature annealing. It is shown that low-temperature annealing in *contaminated* and *contaminant-free* furnaces leads to completely different wettability transitions. Nevertheless, this can be used as an additional approach to obtain the reversibly switchable wettability. As suggested by the experimental results reported in this comment, preheating the furnace to temperatures exceeding 350 °C for several hours can provide a contaminant-free annealing environment. It is also shown that (usually overlooked) contamination may arise from the silicone components of the furnace. In this case, a ToF-SIMS analysis revealed the formation of a thin and homogeneous hydrophobic PDMS film over the whole annealed surface, which can be also recognized by the appearance of the XPS photopeak at 101.8 eV binding energy.

However, heating to 350 °C leads to PDMS oxidation and consequently returns the surface into the initial, super-hydrophilic state.

The theoretical calculations of the reflectivity of a metallic surface covered with thin layer(s) clearly demonstrate that the interference effects should not be neglected to correctly understand and describe its optical properties. Moreover, the presented theoretical calculations also clearly show that controlling the thickness of the laser-induced oxide layer or even the thickness of an additional transparent liquid layer may lead to advanced applications utilizing the switchable optical properties of the laser-textured metallic surfaces.

ASSOCIATED CONTENT

ⓢ Supporting Information

The Supporting Information is available free of charge at https://pubs.acs.org/doi/10.1021/acsami.9b23462.

Additional experimental and theoretical details and figures (PDF)

AUTHOR INFORMATION

Corresponding Author

Peter Gregorčič − *Faculty of Mechanical Engineering, University of Ljubljana, Ljubljana 1000, Slovenia;* ⓘ orcid.org/0000-0003-0459-6369; Phone: +386 1 477 1 172; Email: peter.gregorcic@fs.uni-lj.si

Complete contact information is available at: https://pubs.acs.org/10.1021/acsami.9b23462

Author Contributions

P.G. designed the experiments and calculations, conducted the supplementary experiments and performed the calculations, analyzed and interpreted the presented data, and wrote this comment.

Notes

The author declares no competing financial interest.

ABBREVIATIONS

FIB, focused ion beam

PDMS, polydimethylsiloxane
RoA, roll-of angle
SEM, scanning electron microscope
ToF-SIMS, time-of-flight secondary ion mass spectroscopy
TVOC, total volatile organic compounds
VOC, volatile organic compounds
XPS, X-ray photoelectron spectroscopy

■ REFERENCES

(1) Lian, Z.; Xu, J.; Yu, Z.; Yu, P.; Ren, W.; Wang, Z.; Yu, H. Bioinspired Reversible Switch between Underwater Superoleophobicity/Superaerophobicity and Oleophilicity/Aerophilicity and Improved Antireflective Property on the Nanosecond Laser-Ablated Superhydrophobic Titanium Surfaces. *ACS Appl. Mater. Interfaces* **2020**, *12* (5), 6573−6580.

(2) Kietzig, A. M.; Mirvakili, M. N.; Kamal, S.; Englezos, P.; Hatzikiriakos, S. G. Laser-Patterned Super-Hydrophobic Pure Metallic Substrates: Cassie to Wenzel Wetting Transitions. *J. Adhes. Sci. Technol.* **2011**, *25* (20), 2789−2809.

(3) Xin, B. W.; Hao, J. C. Reversibly switchable wettability. *Chem. Soc. Rev.* **2010**, *39* (2), 769−782.

(4) Alcisto, J.; Enriquez, A.; Garcia, H.; Hinkson, S.; Steelman, T.; Silverman, E.; Valdovino, P.; Gigerenzer, H.; Foyos, J.; Ogren, J.; Dorey, J.; Karg, K.; McDonald, T.; Es-Said, O. S. Tensile Properties and Microstructures of Laser-Formed Ti-6Al-4V. *J. Mater. Eng. Perform.* **2011**, *20* (2), 203−212.

(5) Yang, Z.; Liu, X.; Tian, Y. Insights into the wettability transition of nanosecond laser ablated surface under ambient air exposure. *J. Colloid Interface Sci.* **2019**, *533*, 268−277.

(6) Gregorčič, P.; Conradi, M.; Hribar, L.; Hočevar, M. Long-Term Influence of Laser-Processing Parameters on (Super)hydrophobicity Development and Stability of Stainless-Steel Surfaces. *Materials* **2018**, *11* (11), 2240.

(7) Gregorčič, P.; Šetina-Batič, B.; Hočevar, M. Controlling the stainless steel surface wettability by nanosecond direct laser texturing at high fluences. *Appl. Phys. A: Mater. Sci. Process.* **2017**, *123* (766), 1−8.

(8) McHale, G.; Shirtcliffe, N. J.; Newton, M. I. Super-hydrophobic and super-wetting surfaces: Analytical potential? *Analyst* **2004**, *129* (4), 284−287.

(9) Marmur, A. Hydro- hygro- oleo- omni-phobic? Terminology of wettability classification. *Soft Matter* **2012**, *8* (26), 6867−6870.

(10) Drelich, J.; Chibowski, E.; Meng, D. D.; Terpilowski, K. Hydrophilic and superhydrophilic surfaces and materials. *Soft Matter* **2011**, *7* (21), 9804−9828.

(11) Yan, X.; Huang, Z. Y.; Sett, S.; Oh, J.; Cha, H.; Li, L. N.; Feng, L. Z.; Wu, Y. F.; Zhao, C. Y.; Orejon, D.; Chen, F.; Miljkovic, N. Atmosphere-Mediated Superhydrophobicity of Rationally Designed Micro/Nanostructured Surfaces. *ACS Nano* **2019**, *13* (4), 4160−4173.

(12) Kirner, S. V.; Wirth, T.; Sturm, H.; Krüger, J.; Bonse, J. Nanometer-resolved chemical analyses of femtosecond laser-induced periodic surface structures on titanium. *J. Appl. Phys.* **2017**, *122* (10), 104901.

(13) Veiko, V.; Odintsova, G.; Ageev, E.; Karlagina, Y.; Loginov, A.; Skuratova, A.; Gorbunova, E. Controlled oxide films formation by nanosecond laser pulses for color marking. *Opt. Express* **2014**, *22* (20), 24342−24347.

(14) Łęcka, K. M.; Wójcik, M. R.; Antończak, A. J. Laser-Induced Color Marking of Titanium: A Modeling Study of the Interference Effect and the Impact of Protective Coating. *Math. Probl. Eng.* **2017**, *2017*, 1.

(15) Kietzig, A. M.; Hatzikiriakos, S. G.; Englezos, P. Patterned Superhydrophobic Metallic Surfaces. *Langmuir* **2009**, *25* (8), 4821−4827.

(16) Trdan, U.; Hočevar, M.; Gregorčič, P. Transition from superhydrophilic to superhydrophobic state of laser textured stainless steel surface and its effect on corrosion resistance. *Corros. Sci.* **2017**, *123*, 21−26.

(17) Ta, D. V.; Dunn, A.; Wasley, T. J.; Kay, R. W.; Stringer, J.; Smith, P. J.; Connaughton, C.; Shephard, J. D. Nanosecond laser textured superhydrophobic metallic surfaces and their chemical sensing applications. *Appl. Surf. Sci.* **2015**, *357*, 248−254.

(18) Boinovich, L.B.; Emelyanenko, A.M.; Emelyanenko, K.A.; Domantovsky, A.G.; Shiryaev, A.A. Comment on "Nanosecond laser textured superhydrophobic metallic surfaces and their chemical sensing applications" by Duong V. Ta, Andrew Dunn, Thomas J. Wasley, Robert W. Kay, Jonathan Stringer, Patrick J. Smith, Colm Connaughton, Jonathan D. Shephard (Appl. Surf. Sci. 357 (2015) 248−254). *Appl. Surf. Sci.* **2016**, *379*, 111−113.

(19) Long, J. Y.; Zhong, M. L.; Fan, P. X.; Gong, D. W.; Zhang, H. J. Wettability conversion of ultrafast laser structured copper surface. *J. Laser Appl.* **2015**, *27*, S29107.

(20) Long, J. Y.; Zhong, M. L.; Zhang, H. J.; Fan, P. X. Superhydrophilicity to superhydrophobicity transition of picosecond laser microstructured aluminum in ambient air. *J. Colloid Interface Sci.* **2015**, *441*, 1−9.

(21) Jagdheesh, R.; Diaz, M.; Marimuthu, S.; Ocaña, J. L. Hybrid laser and vacuum process for rapid ultrahydrophobic Ti-6Al-4 V surface formation. *Appl. Surf. Sci.* **2019**, *471*, 759−766.

(22) Yan, H.; Abdul Rashid, M. R. B.; Khew, S. Y.; Li, F.; Hong, M. Wettability transition of laser textured brass surfaces inside different mediums. *Appl. Surf. Sci.* **2018**, *427*, 369−375.

(23) Wang, G. Y.; Zhang, T. Y. Easy Route to the Wettability Cycling of Copper Surface between Superhydrophobicity and Superhydrophilicity. *ACS Appl. Mater. Interfaces* **2012**, *4* (1), 273−279.

(24) Chun, D. M.; Ngo, C. V.; Lee, K. M. Fast fabrication of superhydrophobic metallic surface using nanosecond laser texturing and low-temperature annealing. *CIRP Ann.* **2016**, *65* (1), 519−522.

(25) Ngo, C. V.; Chun, D. M. Fast wettability transition from hydrophilic to superhydrophobic laser-textured stainless steel surfaces under low-temperature annealing. *Appl. Surf. Sci.* **2017**, *409*, 232−240.

(26) Yan, B.; Tao, J. G.; Pang, C.; Zheng, Z.; Shen, Z. X.; Huan, C. H. A.; Yu, T. Reversible UV-light-induced ultrahydrophobic-to-ultrahydrophilic transition in an alpha-Fe2O3 nanoflakes film. *Langmuir* **2008**, *24* (19), 10569−10571.

(27) Ta, V. D.; Dunn, A.; Wasley, T. J.; Li, J.; Kay, R. W.; Stringer, J.; Smith, P. J.; Esenturk, E.; Connaughton, C.; Shephard, J. D. Laser textured superhydrophobic surfaces and their applications for homogeneous spot deposition. *Appl. Surf. Sci.* **2016**, *365*, 153−159.

(28) Strohmeier, B. R. Improving the Wettability of Aluminum Foil with Oxygen Plasma Treatments. *J. Adhes. Sci. Technol.* **1992**, *6* (6), 703−718.

(29) Takeda, S.; Fukawa, M.; Hayashi, Y.; Matsumoto, K. Surface OH group governing adsorption properties of metal oxide films. *Thin Solid Films* **1999**, *339* (1−2), 220−224.

(30) Seshadri, A.; Forrest, E. C.; Shirvan, K. Why ionizing radiation enhances surface wettability. *Appl. Surf. Sci.* **2020**, *514*, 145935.

(31) Rahman, M. M.; Olceroglu, E.; McCarthy, M. Role of Wickability on the Critical Heat Flux of Structured Superhydrophilic Surfaces. *Langmuir* **2014**, *30* (37), 11225−11234.

(32) Wemp, C. K.; Carey, V. P. Water Wicking and Droplet Spreading on Randomly Structured Thin Nanoporous Layers. *Langmuir* **2017**, *33* (50), 14513−14525.

(33) Boinovich, L. B.; Emelyanenko, A. M. Hydrophobic materials and coatings: Principles of design, properties and applications. *Usp. Khim.* **2008**, *77* (7), 619−638.

(34) Biesinger, M. C.; Lau, L. W. M.; Gerson, A. R.; Smart, R. S. C. Resolving surface chemical states in XPS analysis of first row transition metals, oxides and hydroxides: Sc, Ti, V, Cu and Zn. *Appl. Surf. Sci.* **2010**, *257* (3), 887−898.

(35) Rosseler, O.; Sleiman, M.; Montesinos, V. N.; Shavorskiy, A.; Keller, V.; Keller, N.; Litter, M. I.; Bluhm, H.; Salmeron, M.; Destaillats, H. Chemistry of NOx on TiO2 Surfaces Studied by Ambient Pressure XPS: Products, Effect of UV Irradiation, Water, and Coadsorbed K+. *J. Phys. Chem. Lett.* **2013**, *4* (3), 536−541.

(36) Ketteler, G.; Yamamoto, S.; Bluhm, H.; Andersson, K.; Starr, D. E.; Ogletree, D. F.; Ogasawara, H.; Nilsson, A.; Salmeron, M. The

nature of water nucleation sites on TiO2(110) surfaces revealed by ambient pressure X-ray photoelectron spectroscopy. *J. Phys. Chem. C* **2007**, *111* (23), 8278−8282.

(37) Phillips, M. Method for the collection and assay of volatile organic compounds in breath. *Anal. Biochem.* **1997**, *247* (2), 272−278.

(38) Alonso, M.; Castellanos, M.; Martin, B. J.; Sanchez, J. M. Capillary thermal desorption unit for near real-time analysis of VOCs at sub-trace levels. Application to the analysis of environmental air contamination and breath samples. *J. Chromatogr. B: Anal. Technol. Biomed. Life Sci.* **2009**, *877* (14−15), 1472−1478.

(39) Jeong, M. G.; Seo, H. O.; Kim, K. D.; Kim, Y. D.; Lim, D. C. Enhanced photocatalytic activity of TiO2 by polydimethylsiloxane deposition and subsequent thermal treatment at 800 degrees C. *Thin Solid Films* **2012**, *520* (15), 4929−4933.

(40) Glasmastar, K.; Gold, J.; Andersson, A. S.; Sutherland, D. S.; Kasemo, B. Silicone transfer during microcontact printing. *Langmuir* **2003**, *19* (13), 5475−5483.

(41) Ruiz, M. A.; Hernandez, A.; Parera, A.; Gallardo, V. Dimethylsiloxane polymers: Vaporization rate test freezing temperatures. *J. Soc. Cosmet Chem.* **1995**, *46* (3), 175−180.

(42) Ouyang, M.; Yuan, C.; Muisener, R. J.; Boulares, A.; Koberstein, J. T. Conversion of some siloxane polymers to silicon oxide by UV/ozone photochemical processes. *Chem. Mater.* **2000**, *12* (6), 1591−1596.

(43) Yuan, J. K.; Liu, X. G.; Akbulut, O.; Hu, J. Q.; Suib, S. L.; Kong, J.; Stellacci, F. Supporting Information for: Superwetting nanowire membranes for selective absorption. *Nat. Nanotechnol.* **2008**, *3* (6), 332−336.

(44) Abbasi, F.; Mirzadeh, H.; Katbab, A. A. Modification of polysiloxane polymers for biomedical applications: a review. *Polym. Int.* **2001**, *50* (12), 1279−1287.

(45) Born, M.; Wolf, E. *Principles of Optics*; Cambridge University Press: Cambridge, U.K., 2005.

(46) Johnson, P. B.; Christy, R. W. Optical-Constants of Transition-Metals - Ti, V, Cr, Mn, Fe, Co, Ni, and Pd. *Phys. Rev. B* **1974**, *9* (12), 5056−5070.

(47) Skowroński, Ł.; Antończak, A. J.; Trzcinski, M.; Łazarek, Ł.; Hiller, T.; Bukaluk, A.; Wronkowska, A. A. Optical properties of laser induced oxynitride films on titanium. *Appl. Surf. Sci.* **2014**, *304*, 107−114.

(48) Hass, G.; Bradford, A. P. Optical Properties and Oxidation of Evaporated Titanium Films. *J. Opt. Soc. Am.* **1957**, *47* (2), 125−129.

(49) Mash, I. D.; Motulevich, G. P. Optical-Constants and Electron Characteristics of Titanium. *Zh. Eksp. Teor. Fiz.* **1972**, *63* (3), 985−992.

(50) Palik, E. D. *Handbook of Optical Constants of Solids*; Academic Press: New York, 1998.

(51) Tanaka, T. Optical Constants of Polycrystalline 3d Transition-Metal Oxides in the Wavelength Region 350 to 1200 nm. *Jpn. J. Appl. Phys.* **1979**, *18* (6), 1043−1047.

(52) Hale, G. M.; Querry, M. R. Optical-Constants of Water in 200-nm to 200-mum Wavelength Region. *Appl. Opt.* **1973**, *12* (3), 555−563.